Supplementary Information

Mineral physical protection and carbon stabilization in-situ evidence revealed by nano scale 3-D tomography

Yi-Tse Weng[1,#], Chun-Chieh Wang[2,#], Cheng-Cheng Chiang[2],Heng Tsai[3], Yen-Fang Song[2], Shiuh-Tsuen Huang[4], Biqing Liang[1,*]

[1]National Cheng Kung University, Department of Earth Sciences, Tainan, Taiwan ROC

[2]National Synchrotron Resource Research Center, Hsinchu, Taiwan ROC

[3]National Changhua University of Education, Department of Geography, Changhua, Taiwan ROC

[4]National Taichung University of Education, Department of Science Education and Application, Taichung, Taiwan ROC

[#]Equal Contribution

[*]Corresponding author: Biqing Liang

(liangglobalcarbon@gmail.com;liangbq@mail.ncku.edu.tw)

3-D tomography computation and illustration

The final 3-D tomographic structures for visualization and illustration are generated using *Amira* 3-D software for post-image processing (Fig. 1). The

reconstructed datasets first go through *Median* and *Gauss* filter processes to enhance the S/N ratio before 3-D computation. In order to eliminate the noise surrounding the reconstructed datasets, the *LabelField* function is used to define a 3-D mask for specimens of interest. The *Arithmetic* function is used to segment the specimens from surrounding noise according to the 3-D mask. After the above post-image processing, the dataset is illustrated using *Voltex* and *Isosurface*. In general, OC is demonstrated by *Voltex* in proper contrast value, and minerals and gold particles with high intensity are shown by *Isosurface* with a reasonable threshold. Organic C and minerals are bound in the specific spatial region using *SelectRoi*. The *CameraRotate* module is used to show the rotating motion of tomography along a specific axis. The internal structure of specimen is shown under the *clippingPlane* module. The *DemoMaker* module is applied to make an animated sequence of operations for advanced movie recording, and *MovieMaker* is used to export the animated operation to video file.

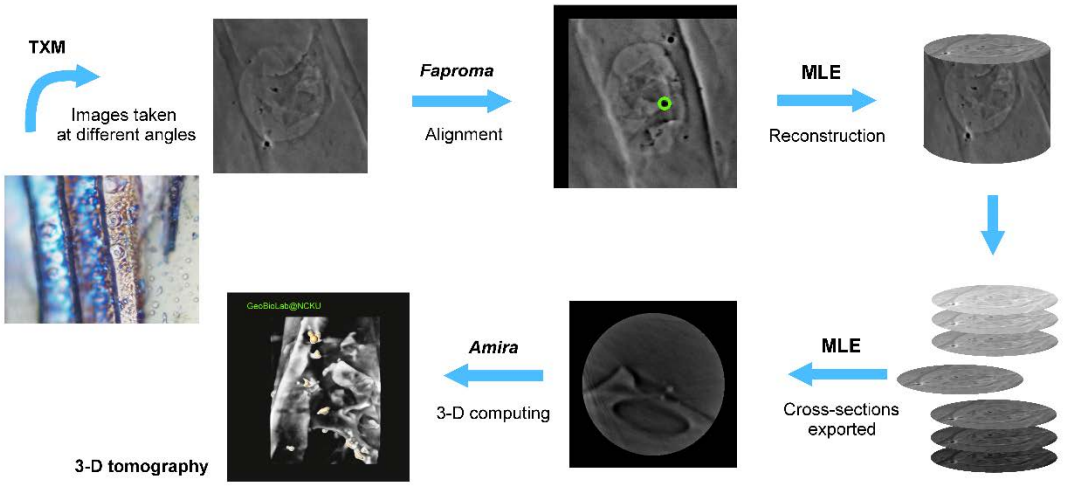

Figure S1. The flowchart for 3-D tomography reconstruction and subsequent 3-D computation for illustration using TXM. Reconstructed 3-D tomography datasets are generated based on measured distribution. And 3-D tomography illustration is generated by image post-process and computation.

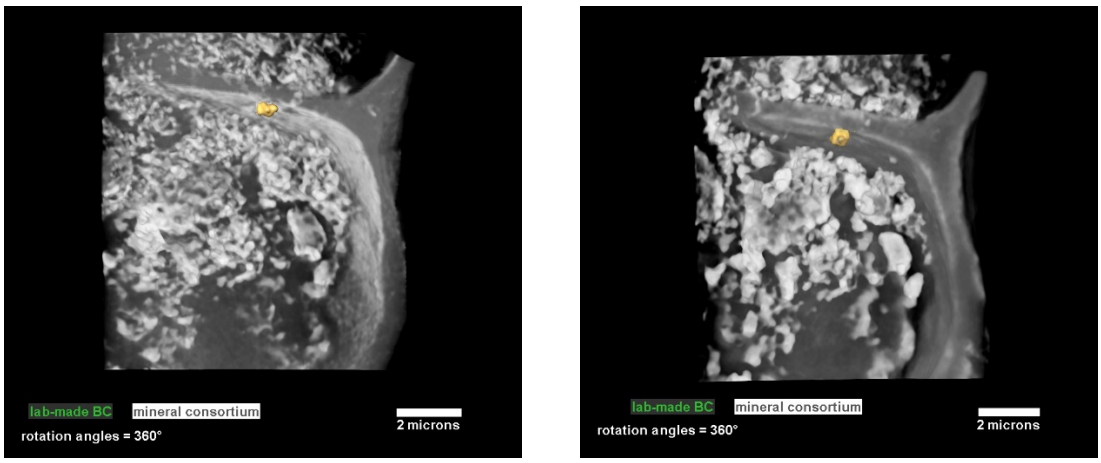

Figure SMOV1. Video illustration extracted from 3-D absorption contrast tomography of lab-made BC and mineral nano particle consortium. Yellow particle is a gold nano particle for position reference. All minerals are shown in silver color. The dark grey part contours the structure and boundary of OC.
https://drive.google.com/open?id=1FD-ui0-lsr4U2eClo6X2AbwqtcuChtII

Figure SMOV2. Video illustration extracted from 3-D phase contrast tomography of lab-made BC and mineral nano particle consortium. Yellow particle is a gold nano particle for position reference. All minerals are shown in silver color. The dark grey part contours the structure and boundary of OC.

https://drive.google.com/open?id=1RglvAplyXrnZTIZQyr7aGTo8vYGbkCJu

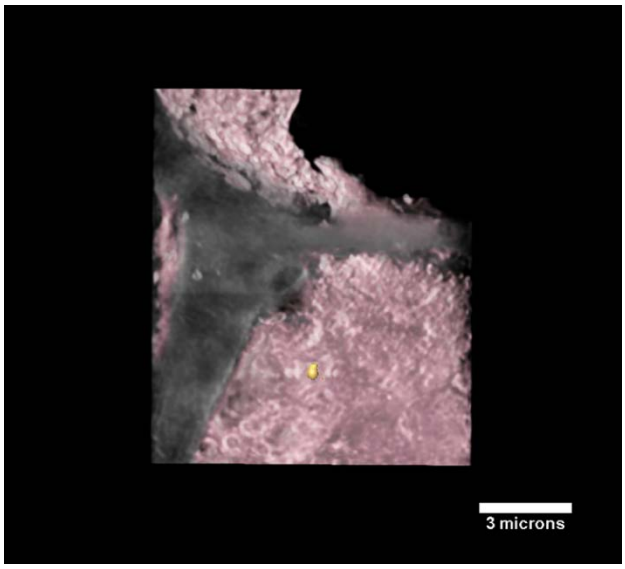

Figure SMOV3. Video illustration obtained from 3-D absorption contrast tomography of high mountain mineral bearing OC. Yellow particle is a gold nano particle for position reference. All minerals are shown in rust color. The dark grey part contours the structure and boundary of OC.

https://drive.google.com/open?id=1-__9KHc3SpncXfuflMy9lQ8V0AIVmB8d

Table S1. XRD peak positions of mineral-bearing OC sample from Mt. Nanhua.

	d (Å)	d-reference (Å)	hkl
Ferrihydrite	2.5644	2.5634	100
	2.2502	2.2504	012
	2.0046	1.9840	013
	1.7344	1.7322	014
	1.5090	1.5160	015
	1.4779	1.4800	110
Goethite	4.9831	5.0000	020
	4.2063	4.2089	110
	2.6992	2.7071	130
	2.5914	2.5913	021
	2.4595	2.4591	111
	2.2625	2.2624	121
	1.7210	1.7284	221
	1.6990	1.7005	240
	1.5650	1.5706	151
	1.5135	1.5150	002
Lepidocrocite	6.2651	6.2700	200
	3.2921	3.2940	210
	2.4747	2.4730	301
	2.4333	2.4340	410
	2.3616	2.3620	111
	1.9402	1.9400	501
	1.9370	1.9350	020
	1.7367	1.7350	511
	1.5333	1.5340	002
	1.5258	1.5240	321
	1.3684	1.3710	521
Quartz	4.2532	4.254	100
	3.3422	3.342	101
	2.4571	2.456	110
	2.2806	2.280	102
	2.2361	2.236	111
	1.9788	1.979	201
	1.8173	1.817	112
	1.6715	1.671	202

	1.5412	1.541	211
	1.3818	1.374	203

Table S2. FTIR peak assignment of mineral-bearing OC sample from Mt. Nanhua.

Wavenumber (cm^{-1})	Model	Reference	Ref. value
1758	Carbonyl C=O stretching	Parikh et al., 2014	1765
1706	Aromatic carbonyl/carboxyl C=O stretching	Özçimen and Ersoy-Meriçboyu, 2010	1709
1596	vC=C in aromatic	Sharma et al., 2004	1597
1454	CH deformation and aromatic ring vibrations	Sharma et al., 2004	1460
1386	Carboxyl C–O symmetric stretching	Parikh et al., 2014	1384
1274	Carboxyl C–O stretching	Parikh et al., 2014	1280
1247	v(C-O) phenolic	Parikh et al., 2014	1240
1113	Si–O stretching	Vaculikova et al., 2011	1113
1062	Si–O stretching	Harsh et al., 2002	1060
1025	Aliphatic ether C–O and alcohol C–O stretching	Parikh et al., 2014	1029
910	OH deformation	Vaculikova et al., 2011	913
875	1 adjacent H deformations	Parikh et al., 2014	870
798	2 adjacent H deformations	Parikh et al., 2014	804
754	4 adjacent H deformations	Parikh et al., 2014	750
694	Fe-OH stretching	Blanch et al. 2008	690
674	In-plane O-H bend	Blanch et al. 2008	670
626	Fe–O stretching	Blanch et al. 2008	633
534	Fe-OH stretching	Blanch et al. 2008	533
497	Fe–O asymmetric stretching	Blanch et al. 2008	497
476	Fe-O vibrations	Parikh et al., 2014	480

(Blanch et al., 2008; Harsh et al., 2002; Özçimen and Ersoy-Meriçboyu, 2010;

Parikh et al., 2014; Sharma et al., 2004; Vaculíková et al., 2011)

References

Blanch, A., Quinton, J., Lenehan, C., and Pring, A.: The crystal chemistry of Al-bearing goethites: An infrared spectroscopic study, Mineral. Mag, 72, 1043-1056, 2008.

Harsh, J., Chorover, J., and Nizeyimana, E.: Allophane and Imogolite, In *Soil Mineralogy with Environmental Applications, SSSA Book Series No. 7*, Edited by:Dixon,J.B. and Schulze,D.G., Madison, WI:SSSA, pp 291–322, 2002.

Özçimen, D. and Ersoy-Meriçboyu, A.: Characterization of biochar and bio-oil samples obtained from carbonization of various biomass materials, Renew. Energy, 35, 1319-1324, 2010.

Parikh, S., W. Goyne, K., Margenot, A., Mukome, F., and J. Calderon, F.: Soil Chemical Insights Provided through Vibrational Spectroscopy, Elsevier, Oxford, pp 1–148, 2014.

Sharma, R. K., Wooten, J. B., Baliga, V. L., Lin, X., Geoffrey Chan, W., and Hajaligol, M. R.: Characterization of chars from pyrolysis of lignin, Fuel, 83, 1469-1482, 2004.

Vaculíková, L., Plevová, E., Vallová, S., and Koutnik, I.: Characterization and differentiation of kaolinites from selected Czech deposits using infrared spectroscopy and differential thermal analysis, Acta Geodyn. Geomater., 8, 59–67. 2011.